JOURNAL OF GEOPHYSICAL RESEARCH, VOL. 99, NO. B11, PAGES 21,947–21,961, NOVEMBER 10, 1994

Excitation of atmospheric oscillations by volcanic eruptions

Hiroo Kanamori
Seismological Laboratory, California Institute of Technology, Pasadena

Jim Mori
U.S. Geological Survey, Pasadena, California

David G. Harkrider
Seismological Laboratory, California Institute of Technology, Pasadena

Abstract. We investigated the mechanism of atmospheric oscillations with periods of about 300 s which were observed for the 1991 Pinatubo and the 1982 El Chichón eruptions. Two distinct spectral peaks, at T=270 and 230 s for the Pinatubo eruption and at T=195 and 266 s for the El Chichón eruptions, have been reported. We found similar oscillations for the 1980 Mount St. Helens and the 1883 Krakatoa eruptions. To explain these observations, we investigated excitation problems for two types of idealized sources, "mass injection" and "energy injection" sources, placed in an isothermal atmosphere. In general, two modes of oscillations, "acoustic" and "gravity" modes, can be excited. For realistic atmospheric parameters, the acoustic and gravity modes have a period of 275 and 304 s, respectively. For a realistic time history of eruption, atmospheric oscillations with an amplitude of 50 to 100 Pa (0.5 to 1 mbar) can be excited by an energy injection source with a total energy of 10^{17} J. This result is consistent with the observations and provides a physical basis for interpretation of atmospheric oscillations excited by volcanic eruptions.

Introduction

Kanamori and Mori [1992] and *Widmer and Zürn* [1992] observed an unusually long (at least 3 hours) Rayleigh wave train having periods of about 230 and 270 s during the eruption of Mount Pinatubo. *Kanamori and Mori* [1992] interpreted this as Rayleigh waves excited near the volcano by atmospheric oscillations set up by the eruption, as schematically shown in Figure 1. The thermal energy emitted by eruption can continuously excite two types of atmospheric oscillations, "acoustic" and "gravity" modes. *Harkrider* [1964], *Press and Harkrider* [1962], and *Pfeffer and Zarichny* [1963] computed dispersion curves of air waves for many models of the Earth's atmosphere. These dispersion curves show two group velocity minima at periods of about 250 s, the proximity of which to those of the two observed spectral peaks suggests that atmospheric oscillations excited near these periods transferred the energy to the ground and excited the Rayleigh waves. *Widmer and Zürn* [1992] also identified a similar oscillation with periods of 195 and 266 s for the 1982 El Chichón, Mexico, eruption. They preferred an interpretation that some feedback between local atmospheric oscillations and the eruption process regulated the oscillation period.

Although the interpretation shown in Figure 1 appears qualitatively reasonable, it is unclear whether the proposed mechanism can explain the observations quantitatively. The two characteristic frequencies, ω_a and ω_b, are cutoff frequencies and do not necessarily imply resonance at these frequencies. It is also desirable to demonstrate that the thermal energy of the eruption was sufficient to excite the observed oscillations.

The main purpose of this paper is to provide a physical basis to the model proposed by *Kanamori and Mori* [1992]. Many investigations of atmospheric waves excited by volcanic eruptions have been made [*Blanc*, 1985]. *Pekeris* [1948a, b], *Press and Harkrider* [1962], and *Harkrider and Press* [1967] studied atmospheric waves excited by the eruption of Krakatoa in 1883, and *Bolt and Tanimoto* [1981] and *Mikumo and Bolt* [1985] analyzed the air waves excited by the 1980 eruption of Mount St. Helens. These studies are on the far-field Lamb pulse, and no investigation has been made on atmospheric oscillations near the source, because such oscillations had not been observed before the 1991 Pinatubo eruption. A spectral feature similar to that observed for the Pinatubo eruption has been observed for ionospheric waves excited by severe storms. *Jones and George* [1976] explained this feature in terms of resonant interactions between the waves and atmospheric temperature structure.

Paper number 94JB01475.
0148-0227/94/94JB-01475$05.00

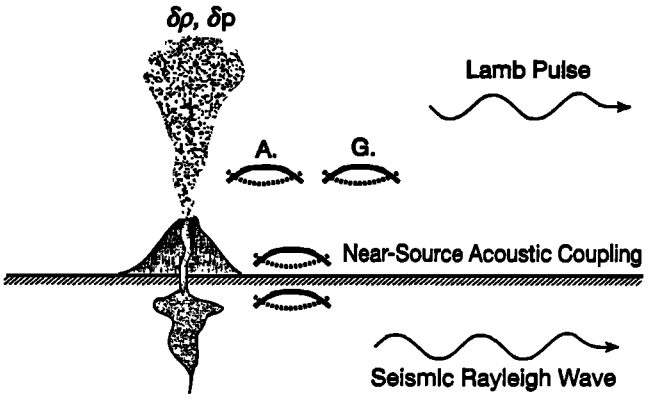

Figure 1. Schematic diagram showing the excitation mechanism of atmospheric oscillations by a volcanic eruption and acoustic coupling of atmospheric oscillations to seismic Rayleigh waves. The thermal energy emitted by an eruption excites "acoustic" and "gravity" modes of atmospheric oscillations. The energy is then coupled to the ground near the source, which excites seismic Rayleigh waves.

We will show that near-source excitation of atmospheric oscillations at periods of about 300 s is physically feasible for a reasonable model of volcanic eruptions.

Summary of Observations

Figure 2a shows the three-component very long period (VLP) seismograms recorded at MAJO (Matsushiro, Japan) during the Pinatubo eruption. The unusual long-period wave train recognized by *Kanamori and Mori* [1992] as the signature of the Pinatubo atmospheric oscillations is indicated by P. Symbols E_1 and E_2 indicate earthquakes in the Caucasus (M=6.3), and the South Sandwich Islands (M=6.5), respectively. Symbols E_3 and E_4 indicate two earthquakes (M=5.5 and 5.3, respectively) in the Philippines associated with the Pinatubo eruption. Figure 2b shows a portion (from 4 to 10 hours) of the vertical component with an expanded vertical scale. An almost harmonic wave train is clearly shown. Figure 2c shows the spectrum of the wave train from 0500 to 1000 UT. The spectrum indicates that the wave train is almost harmonic with a dominant peak at 228 s (0.0044 Hz) and minor peak at about 270 s (0.0037 Hz). The latter peak is not much higher than other minor peaks, but *Widmer and Zürn* [1992] demonstrated that this peak was consistently observed at many stations. *Widmer and Zürn* [1992] observed these oscillations with a gravity meter at the Black Forest Observatory, Germany. From this record as well as those from 13 International Deployment of Accelerometers (IDA) stations, they determined the periods to be 225 and 272 s. *Widmer and Zürn* [1992] performed a similar analysis of nine IDA records for the 1982 El Chichón, Mexico, eruption and found spectral peaks at 195 and 270 s.

For the 1980 Mount St. Helens eruption, *Kanamori and Given* [1982] and *Kanamori et al.* [1984] analyzed long-period surface waves, but they did not find any evidence for

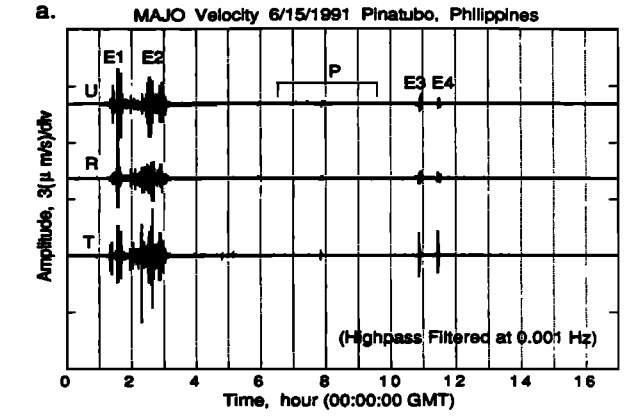

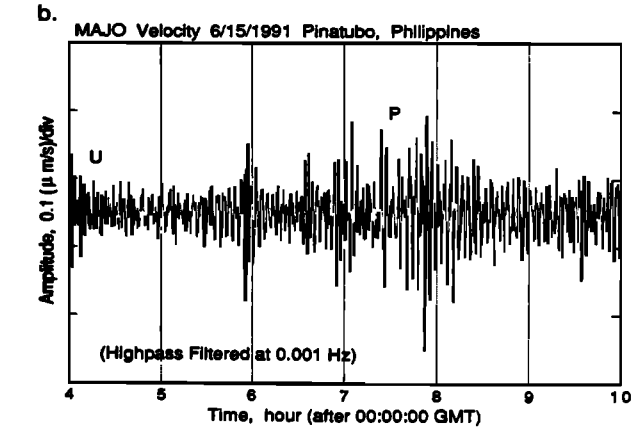

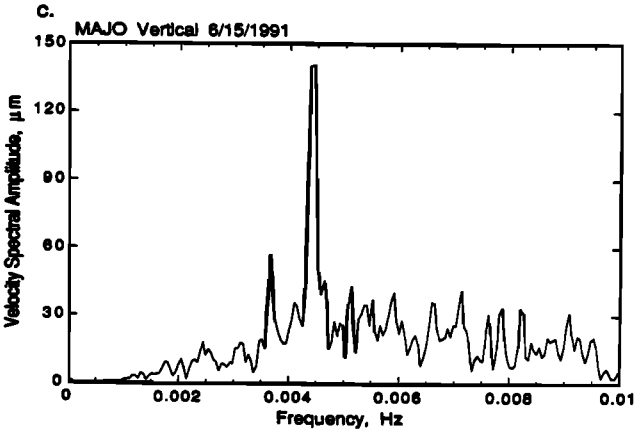

Figure 2. (a) The three-component (vertical and two horizontal components rotated in radial and transverse directions with respect to the Philippines) very long period (VLP) seismograms recorded at Matsushiro, Japan (MAJO) (Δ=26.4°). E_1 and E_2 indicate earthquakes in the Caucasus (M=6.3) and the South Sandwich Islands (M=6.5), respectively. E_3 and E_4 indicate two earthquakes (M=5.5 and 5.3, respectively) in the Philippines associated with the Pinatubo eruption. The long-period wave train excited by the Pinatubo eruption is indicated by P. (b) Enlarged plot of the vertical component shown in Figure 2a. (c) The spectrum of the vertical component of the MAJO record shown in Figure 2a. The time window used is from 0500 to 1000 UT.

such oscillations. We reanalyzed a long-period Global Digital Seismic Network (GDSN) seismogram recorded at Longmire (LON), only 67 km away from Mount St. Helens, and found a distinct oscillation at a period of 300 s (Figure 3). *Kanamori and Given* [1983] earlier analyzed this particular record and found that the seismometer at LON was actually functioning as a barograph rather than seismograph. They interpreted the seismogram as the response of the seismometer to changes in density caused by air waves. Using the same method as that used by *Kanamori and Given* [1983], we estimated the pressure amplitude of the 300 s wave recorded at LON to be about 30 Pa (0.3 mbar). This pressure is about 1/10 of that observed for the Pinatubo eruption.

Another interesting example is found for the 1883 Krakatoa eruption. A barograph record obtained at Batavia (now Jakarta), about 200 km away from the Krakatoa summit, showed distinct oscillations with a period of about 300 s, as shown in Figure 4, which is taken from *Simkin and Fiske* [1983]. Because of the low quality of the record, this oscillation has not been given any serious attention.

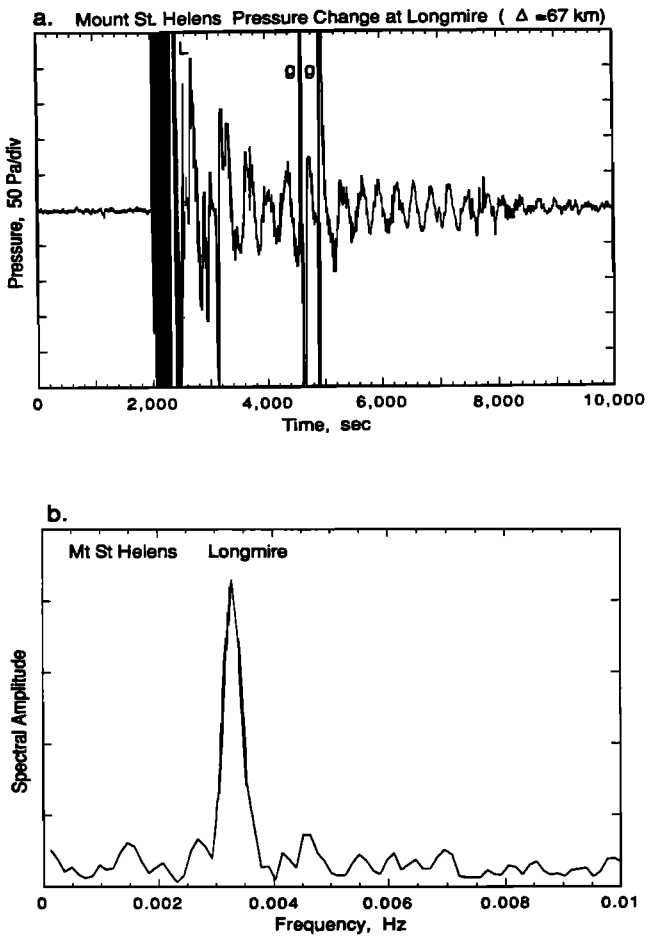

Figure 3. The Global Digital Seismographic Network (GDSN) long-period seismogram of the 1980 Mount St. Helens eruption recorded at station Longmire (Δ=67 km). The large pulse labeled L near the beginning of the record (clipped on the plot shown) is the Lamb pulse. The two spikes labeled g at about 2500 s after the eruption are instrumental glitches. The spectrum shown below is computed for the record section after these glitches.

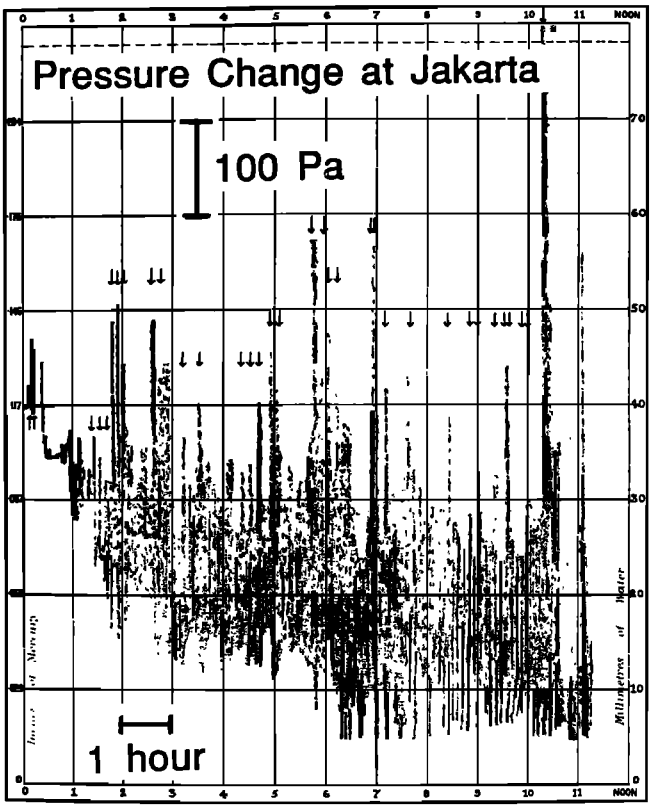

Figure 4. The barograph record at Jakarta (then Batavia, Δ=200 km) of the 1883 Krakatoa eruption [from *Simkin and Fiske*, 1983]. The regular stripe pattern seen on the record suggests atmospheric oscillations. For the record section from 8 to 10 hours, approximately 10 to 12 stripes can be counted for each hour. This indicates oscillations with a period of about 300 s.

However, in view of our observation of the Pinatubo eruption, we are convinced that this oscillation is of the same kind as that observed during the Pinatubo eruption. The pressure amplitude is at least 200 Pa (2 mbar) (the later part of the record is clipped).

These results are summarized in Table 1. Considering these observations, we conclude that excitation of atmospheric oscillations with periods of about 300 s is fairly common.

Theory

We consider a simple problem of free oscillations of isothermal (temperature T_0) atmosphere under constant gravity, g. Although the isothermal atmosphere is simple, its density stratification caused by gravity provides the key mechanism for excitation and propagation of acoustic waves and internal gravity waves; it is useful for understanding how the two characteristic frequencies, ω_a and ω_b, control the near-source oscillations. In the lower part of the Earth's atmosphere, the temperature gradient, about 6.5°K km^{-1}, is smaller than the adiabatic lapse rate, about 10°K km^{-1}, and the difference provides buoyancy necessary for generation of internal gravity waves. If we are to investigate the Lamb pulse at far field, however, it is

Table 1. Atmospheric Oscillations Excited by Volcanic Eruptions

Eruption	Period	Amplitude	References
1991 Pinatubo	270 s, 230 s	300 Pa (3 mbar) (at 30 km)	*Kanamori and Mori* (1992) *Widmer and Zürn* (1992)
1982 El Chichón	195 s, 266 s		*Widmer and Zürn* (1992)
1980 Mount St. Helens	≈300 s	30 Pa (0.3 mbar) (at 67 km)	this study
1883 Krakatoa	≈300 s	>200 Pa (2 mbar) (at 200 km)	this study

essential to introduce realistic boundary conditions and atmosphere models.

The basic theory is given by *Lamb* [1932, p. 541] For purposes of presenting our method, here we recapitulate the basic theory.

We take a Cartesian coordinate system (x, y, z), with the z axis taken upward vertical. We write the x, y, and z components of the velocity field measured from the background state by u, v, and w, respectively. The pressure and density are written as p_0+p and $\rho_0+\rho$, where p_0 and ρ_0 represent the background states and p and ρ, the perturbations from them.

Then the equations of state and hydrostatic equilibrium are given by

$$p_0 = \rho_0 R_g T_0$$
$$\frac{\partial p_0}{\partial z} = -g\rho_0 \tag{1}$$

where R_g is the gas constant of the air. Then p_0 and ρ_0 are given by

$$p_0(z) = p_0(0)\exp(-gz/R_gT_0) \tag{2}$$

and

$$\rho_0(z) = \rho_0(0)\exp(-gz/R_gT_0) \tag{3}$$

In an isothermal atmosphere, the sound velocity c and the scale height H_S are independent of z and are given by

$$c^2 = \gamma p_0/\rho_0 = \gamma R_g T_0 \tag{4}$$

and

$$H_S = R_g T_0/g \tag{5}$$

where γ is the specific heat ratio.

The linearized equations for conservation of momentum, mass, and energy are given by

$$\rho_0\frac{\partial u}{\partial t} = -\frac{\partial p}{\partial x}$$
$$\rho_0\frac{\partial v}{\partial t} = -\frac{\partial p}{\partial y} \tag{6}$$
$$\rho_0\frac{\partial w}{\partial t} = -\frac{\partial p}{\partial z} - \rho g$$

$$\frac{\partial \rho}{\partial t} + w\frac{\partial \rho_0}{\partial z} + \rho_0\left(\frac{\partial u}{\partial x}+\frac{\partial v}{\partial y}+\frac{\partial w}{\partial z}\right) = 0 \tag{7}$$

and

$$\frac{\partial p}{\partial t} - g\rho_0 w = c^2\left(\frac{\partial \rho}{\partial t} + w\frac{\partial \rho_0}{\partial z}\right) \tag{8}$$

respectively [e.g., *Houghton*, 1986, p. 105; *Gill* 1982, p. 170].

From the first two equations of (6), and using equations (7) and (8), we obtain

$$\rho_0\frac{\partial}{\partial t}\left(\frac{\partial w}{\partial z} - \frac{g}{c^2}w\right) = \left(\frac{\partial^2}{\partial x^2}+\frac{\partial^2}{\partial y^2}-\frac{1}{c^2}\frac{\partial^2}{\partial t^2}\right)p \tag{9}$$

Eliminating ρ from the third equation of (6) and equation (8), we obtain

$$\frac{\partial^2 w}{\partial t^2} - g\left(\frac{1}{\rho_0}\frac{\partial \rho_0}{\partial z} + g\frac{1}{c^2}\right)w = -\frac{1}{\rho_0}\frac{\partial}{\partial t}\left(\frac{\partial p}{\partial z} + \frac{g}{c^2}p\right) \tag{10}$$

Plane Wave

We first consider a two-dimensional wave propagation on x-z plane. Assuming the dependence of u, w, p/p_0, and ρ/ρ_0 on x, z, and t in the form

$$\exp(az)\exp[i(\omega t+kx+mz)] \tag{11}$$

and substituting this in the linearized equations, we obtain

$$a = 1/2H_S \tag{12}$$

and a physical dispersion relation

$$m^2 = k^2\left(\frac{\omega_b^2}{\omega^2}-1\right) + \frac{\left(\omega^2-\omega_a^2\right)}{c^2} \tag{13}$$

where

$$\omega_b^2 = \frac{(\gamma-1)g}{\gamma H_S} \tag{14}$$

and

$$\omega_a^2 = \frac{\gamma g}{4H_S} = \left(\frac{c}{2H_S}\right)^2 \tag{15}$$

The angular frequencies ω_a and ω_b are the acoustic cut off and the Brunt-Väisälä frequencies [*Brunt*, 1927; *Väisälä*, 1925], respectively. If c=300 m/s, then H_S=6.6 km, ω_a=0.0229 s^{-1}, and ω_b=0.0207 s^{-1}, with the corresponding periods of 275 and 304 s, respectively.

Now we consider a plane wave propagating vertically along the z axis, i.e., k=0. If $\omega>\omega_a$, m in (13) is real, and (11) represents a vertically propagating wave. If $\omega_a>\omega>0$, m is a pure imaginary, and (11) represents an oscillation with angular frequency ω. This result agrees with that of *Lamb* [1932], who solved the problem in a different way. Using (11) and (13), we can show that if the atmosphere is excited by a horizontal planar pressure source $p_s \exp(i\omega t)$ at z=0,

$$w = \frac{i\omega c}{2\gamma\left(\omega_a^2 - \omega^2\right)^{1/2}}[p_s / p_0(0)] \cdot \exp\left\{\left[\frac{\omega_a}{c} \mp \frac{1}{c}\left(\omega_a^2 - \omega^2\right)^{1/2}\right] z\right\} \exp(i\omega t) \tag{16}$$

and resonance occurs at $\omega=\omega_a$.

This result appears to support the conclusion of *Kanamori and Mori* [1992] that the dominant peak observed for the Pinatubo eruption corresponds to this oscillation with the acoustic cut off frequency.

Equation (12) indicates that u, w, p/p_0, and ρ/ρ_0 increase with z as $\exp(z/2H_S)$ which may look somewhat strange. However, this is physically reasonable, because the energy density is proportional to $\rho_0^{1/2}u$, $\rho_0^{1/2}w$, and $\rho_0^{-1/2}p$ [*Gill*, 1982, p. 171]. Since $\rho_0 \propto \exp(-z/H_S)$ the energy is bounded. However, for z much larger than the scale height H_S, the linear theory is no longer valid.

Point Source

The situation is somewhat different for a point source. Because the wave energy propagates away from the source, the above resonance does not necessarily occur.

The point source problem has been studied by *Weston* [1961a, b], *Row* [1967] *Pierce* [1963], *Ben-Menachem and Singh* [1981] and D. Harkrider (unpublished note, 1975). Here we consider two types of sources, "mass injection" and "energy injection" sources. The "mass injection" source is given by

$$4\pi F_M \exp(i\omega t)\delta(\bar{R} - \bar{R}_s) \tag{17}$$

to be added to the right-hand side of the equation for mass conservation (equation (7)). Here $\bar{R}_s = (0, 0, z_s)$ is the location of the point source, and F_M is the mass injected per unit time. Similarly, the "energy injection" source is given by

$$4\pi F_E \exp(i\omega t)\delta(\bar{R} - \bar{R}_s) \tag{18}$$

to be added to the right-hand side of the energy equation (8). Here F_E is the energy injected per unit time. The solutions for a point source is given in Appendix A.

A volcanic eruption injects both mass and thermal energy. The mass injection source represents injection of net mass and affects ρ only. Injection of energy affects both ρ through thermal expansion and p through compressibility. If we denote the heat injected per unit mass by δq, then

$$\delta q = -\frac{c^2}{(\gamma-1)}\frac{1}{\rho}d\rho + \frac{1}{\rho(\gamma-1)}dp \tag{19}$$

Thus if dp=0, then the energy injection source is equivalent to the mass injection source except for the constant factor $c^2/(\gamma$-1). However, in general, $dp\neq0$, and the energy injection source and the mass injection source have different effects on excitation. As shown below, the solution for the mass injection source is much simpler than that for the energy injection source for which the solution can be obtained only for a special case.

Point Mass Injection Source

From (A12) in Appendix A,

$$p(r,z,t) = i\omega F_M \exp\left(-\frac{z-z_s}{2H_s}\right) \cdot \frac{(\omega^2-\omega_b^2)^{1/2}}{(\omega^2-\omega_c^2)^{1/2}}\frac{1}{R}\exp\left[i\omega\left(t \pm \frac{R}{C}\right)\right] \tag{20}$$

where

$$R^2 = r^2 + (z-z_s)^2$$

$$r^2 = x^2 + y^2$$

$$\omega_c = \frac{|z-z_s|}{R}\omega_b$$

and

$$C = \frac{c\omega(\omega^2-\omega_b^2)^{1/2}}{(\omega^2-\omega_c^2)^{1/2}(\omega^2-\omega_a^2)^{1/2}} \tag{21}$$

The plus or minus sign in (20) should be chosen to satisfy the radiation and causality conditions (see Appendix B).

For an observer at r=0, $\omega_c=\omega_b$, and we obtain

$$p(0,z,t) = i\omega F_M \exp\left(-\frac{z-z_s}{2H_s}\right)\frac{1}{R}\exp\left[i\omega\left(t \pm \frac{R}{C}\right)\right] \tag{22}$$

where

$$C = \frac{c\omega}{(\omega^2-\omega_a^2)^{1/2}} \tag{23}$$

For a mass injection source which varies as a step function, the pressure change can be computed by

integration of (20) with ω. When r=0, the integral can be obtained in a closed form as [*Row*, 1967]

$$p_H(0,z,t) = \frac{1}{2\pi|z-z_s|} F_M \exp\left(-\frac{z-z_s}{2H_s}\right) \cdot \int_{-\infty}^{+\infty} \exp\left\{i\left[\omega t \pm t_0\left(\omega^2-\omega_a^2\right)^{1/2}\right]\right\} d\omega$$

$$= \frac{1}{|z-z_s|} F_M \exp\left(-\frac{z-z_s}{2H_s}\right) \cdot \left\{\delta(t-t_0) - \frac{\omega_a t_0 J_1\left[\omega_a (t^2-t_0^2)^{1/2}\right]}{(t^2-t_0^2)^{1/2}} H(t-t_0)\right\} \quad (24)$$

where t_0=R/c. The first term in the braces (delta function) represents the direct pulse. Since

$$J_1(\xi) \propto \sqrt{\frac{2}{\pi\xi}} \cos\left(\xi - \frac{3}{4}\pi\right)$$

for large ξ, the second term represents an oscillation with the angular frequency ω_a, the acoustic cut off frequency, at large t.

Figure 5a shows this oscillation for a step function mass injection source with a rate of 10^9 kg/s. The source is at a height of 5 km, and the pressure change at r=z=0 is computed. The spectrum of the pressure variation shown in Figure 5a of course yields a single peak at ω=ω_a, as shown in Figure 5b.

For an observer at an arbitrary point we must evaluate the integral

$$p_H(r,z,t) = \frac{1}{2\pi} F_M \exp\left(-\frac{z-z_s}{2H_s}\right) \cdot \int_{-\infty}^{+\infty} \frac{(\omega^2-\omega_b^2)^{1/2}}{(\omega^2-\omega_c^2)^{1/2}} \frac{1}{R} \exp\left[i\omega\left(t \pm \frac{R}{C}\right)\right] d\omega \quad (25)$$

where C is given by (21). This integral involves three branch points at ω=ω_a, ω_b, and ω_c, and no closed form expression is available. We evaluated this integral numerically (see Appendix B for details), and the results are shown in Figures 5c and 5e. The waveform is more complicated than that for r=0, because the branch points at ω=ω_a, ω_b, and ω_c are responsible for excitation of oscillations at these frequencies. Figures 5d and 5f show the corresponding spectra.

The results shown in Figure 5 can be interpreted as follows. At r=0, only the acoustic mode can be observed (Figures 5a and 5b). From the dispersion relation (13), we obtain ω=ω_a when k=0, and m=0. As shown by (16) this corresponds to an acoustic vertical oscillation. From (13), we can show that the horizontal phase velocity is ∞ and the group velocity is 0 for this oscillation. The absence of a peak at ω=ω_b may be somewhat counterintuitive because one would expect vertical oscillation of a parcel of air at ω=ω_b near the source. However, for vertical buoyancy oscillation in isothermal atmosphere the horizontal and vertical pressure gradients vanish, resulting in no pressure perturbation (Figure 6a). Even if a rigid surface and a temperature stratification are included in the model, we suspect that the pressure perturbation at ω=ω_b would be very small at r=0, because of the very nature of the internal wave illustrated in Figure 6.

At r=(z_S-z) (Figures 5c and 5d), the oscillation with ω=ω_c dominates. This is exactly what is expected for internal gravity waves as illustrated in Figure 6b. For internal gravity waves the phase velocity vector and group velocity vector are approximately perpendicular to each other; they are exactly perpendicular for incompressible fluid [*Gill*, 1982, p. 131]. The oscillation is in the direction of the group velocity vector. Thus at point P, the dominant frequency is determined by oscillation in the direction of SP. Since the component of gravity in this direction is $g\cos\phi$=$g(z_S$-$z)/R$, the dominant frequency of the gravity mode to be observed at this point is ω_c=$\omega_b\cos\phi$. Our result (Figure 5d) shows a dominant peak at ω=ω_c, as expected, with smaller peaks at ω≈ω_a and ω_b. The acoustic mode at ω≈ω_a can be explained in the same way as that at r=0. However, the peak at ω=ω_b cannot be explained by the simple geometry shown in Figure 6b. We suggest that when the step function mass injection is given at S, the mode at ω=ω_b is preferentially excited at the source, and the energy is carried by either acoustic or gravity wave. At a large distance, r=6(z_S-z), the mode at ω=ω_c becomes very long period, leaving only the two peaks at ω=ω_b and ω=ω_a in the frequency band of our interest, as shown in Figure 5f.

Figure 7 shows the spectra at various distances (i.e., various ϕ) and illustrates the situation described above. In general, the gravity mode with ω=ω_c dominates, and the peaks at ω=ω_a and ω_b are relatively minor. However, the peaks at ω=ω_a and ω_b, though minor, are always at about the same frequency regardless of ϕ but ω_c varies with ϕ very rapidly. Thus when the source has some vertical extent, or the air wave energy is coupled to the ground over some distance around the source, the mode at ω=ω_c will not show up as a distinct peak, but the modes at ω=ω_a and ω_b yield a distinct spectral peak.

The ratio ω_b/ω_a is about 0.9 for an isothermal atmosphere so that two nearby spectral peaks are expected. The peaks at 230 and 270 s observed for the 1991 Pinatubo eruption correspond to the oscillations at these frequencies. The difference between the ratio of the observed periods and of the computed periods is not surprising considering the difference between the real atmosphere and the simple model used here.

Inclusion of the Earth's surface at z=0 would not affect the above conclusion significantly but would yield a surface wave which propagates at velocity c (Lamb wave). The Earth's surface requires the rigid boundary condition for atmosphere, w=0 at z=0, which, for a horizontally propagating plane wave, requires w to vanish at all z [*Pekeris*, 1948b]. In this case, from equation (9), p is a solution of a wave equation, and a nondispersive pressure wave propagates horizontally at the sound velocity c. From equation (10), we see that the amplitude of a Lamb wave decays as exp(-$H_S z/\gamma$) as the altitude increases. In the

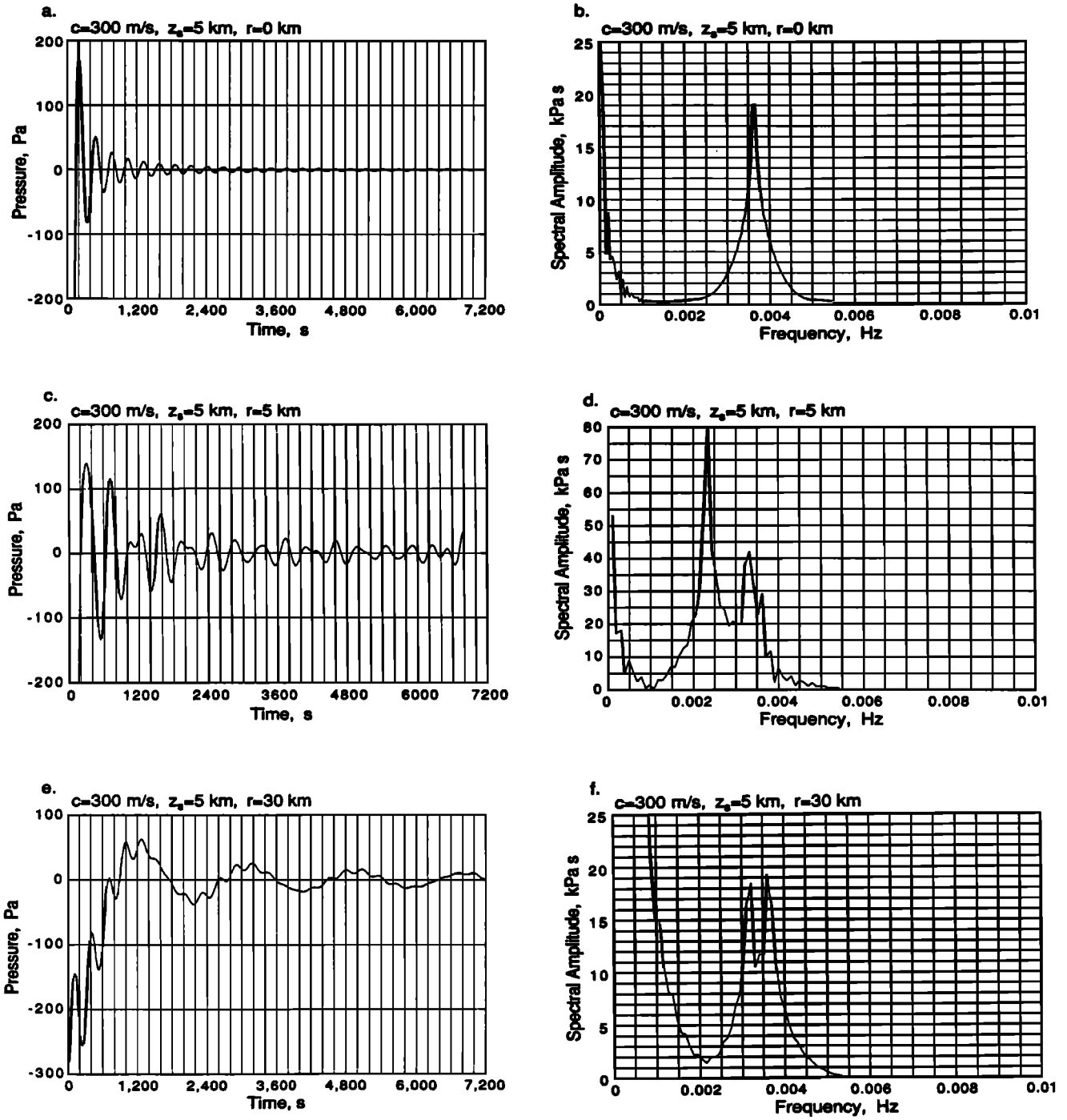

Figure 5. Pressure changes and their spectra computed for a mass injection source with a constant rate of 10^9 kg/s, placed at an altitude of 5 km. (a) Pressure change at r=0 km. (b) Spectrum of Figure 5a. (c) Pressure change at r=5 km. (d) Spectrum of Figure 5c. (e) Pressure change at r=30 km. (f) Spectrum of Figure 5e.

Earth's atmosphere, the sound velocity varies as a function of z so that a Lamb wave exhibits dispersion. The Lamb wave from an impulsive source such as large atmospheric explosions and volcanic eruptions exhibits an Airy function-like waveform [*Gill*, 1982, p. 178]. The Lamb pulse which becomes important at large distances has been observed for many eruptions and has been extensively studied [e.g., *Pekeris*, 1948a, b; *Harkrider and Press*, 1967; *Mikumo and Bolt*, 1985].

The waves discussed in this paper are not Lamb waves but the acoustic and internal gravity waves observed primarily in the near-source region. At large distances, these waves become less important compared with the Lamb wave [*Gill*, 1982, p. 177].

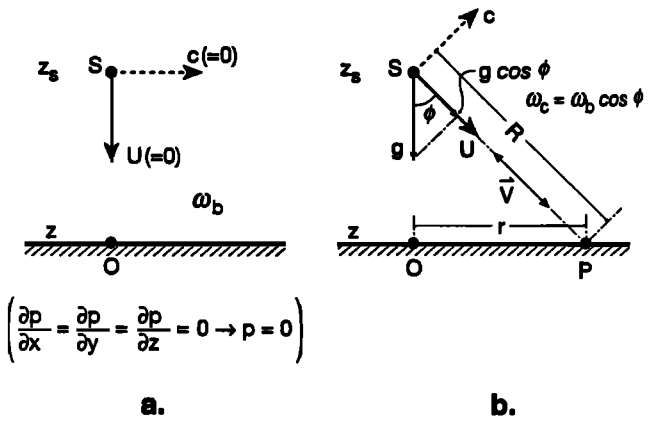

Figure 6. Schematic diagram showing propagation of internal gravity waves.

Point Energy Injection Source

From (A13) of Appendix A, we obtain a particular solution

$$p(r,z,t)=\frac{i\omega F_E}{c^2}\exp\left(-\frac{z-z_s}{2H_s}\right)\frac{1}{R}\exp\left[i\omega\left(t\pm\frac{R}{C}\right)\right]$$
$$\cdot\left[\frac{\omega^2}{(\omega^2-\omega_b^2)^{1/2}(\omega^2-\omega_c^2)^{1/2}}\left(1-\frac{g}{2\omega^2H_s}\right)\right.$$
$$\left.-\frac{g(z-z_s)}{cR}\frac{(\omega_a^2-\omega^2)^{1/2}}{(\omega^2-\omega_c^2)}-\frac{g(z-z_s)}{R^2}\frac{(\omega^2-\omega_b^2)^{1/2}}{(\omega^2-\omega_c^2)^{3/2}}\right] \quad (26)$$

This solution is equivalent to equation (9.246) of *Ben-Menachem and Singh* [1981]. To obtain a step function response we must integrate (26) with ω, but the integral cannot be evaluated easily for the general case. Here we consider only the case for $z=z_S$ and $r\neq 0$ in which (26) can be greatly simplified as

$$p(r,z,t)=\frac{i\omega F_E}{c^2}\frac{1}{R}\left[\frac{\omega}{(\omega^2-\omega_b^2)^{1/2}}\left(1-\frac{g}{2\omega^2H_s}\right)\right]$$
$$\cdot\exp\left[i\omega\left(t\pm\frac{R}{C}\right)\right] \quad (27)$$

where

$$C=\frac{c(\omega^2-\omega_b^2)^{1/2}}{(\omega^2-\omega_a^2)^{1/2}} \quad (28)$$

For a step function source,

$$p_H(r,z,t)=\frac{F_E}{2\pi c^2R}\int_{-\infty}^{+\infty}\frac{\omega}{(\omega^2-\omega_b^2)^{1/2}}\left(1-\frac{g}{2\omega^2H_s}\right)$$
$$\cdot\exp\left[i\omega\left(t\pm\frac{R}{C}\right)\right]d\omega \quad (29)$$

We carried out integration numerically (see Appendix B), and the result is shown in Figure 8. As is expected from the integrand of (29), the spectrum is dominated by a peak at ω_b, with a minor peak at ω_a. The peak at ω_a is due to contribution from C given by (28).

We can compare Figure 8 with Figure 5 as follows. If we use equation (19) and assume dp=0, the mass injection source with F_M is equivalent to an energy injection source with $F_E \cdot c^2/(\gamma-1)$. Thus Figure 5 should correspond to that for an energy injection source with F_E=2.25x10^{14} J/s.

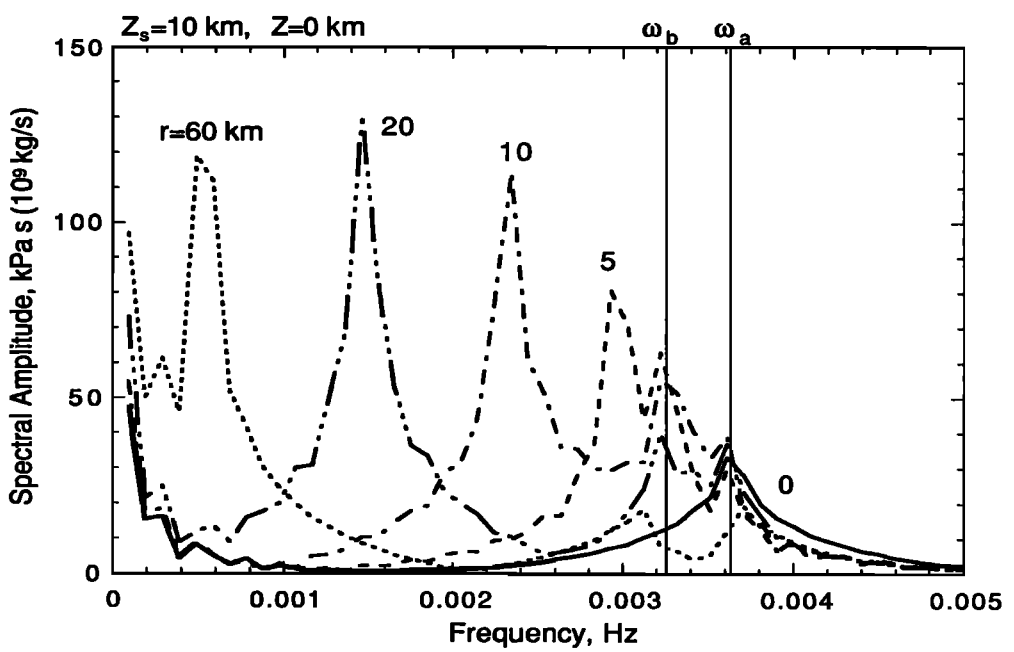

Figure 7. Spectra of pressure changes at various distances from the source. The two vertical lines indicate $\omega=\omega_a$ and $\omega=\omega_b$.

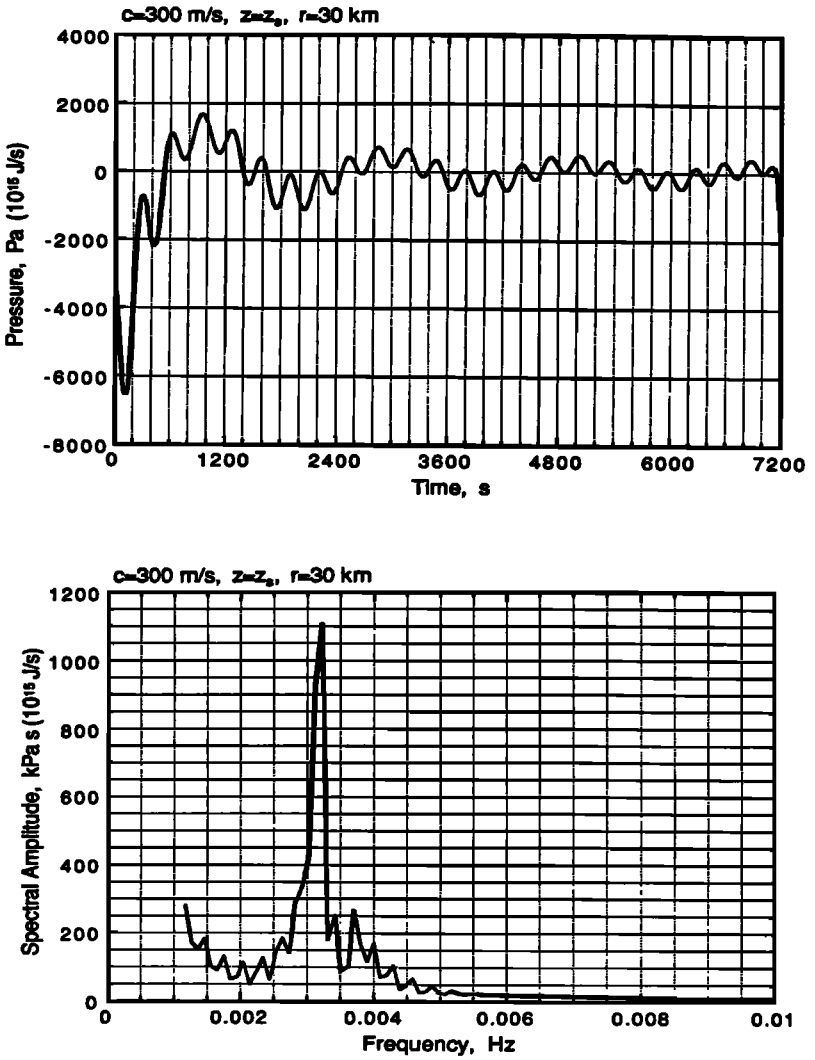

Figure 8. Pressure change and its spectrum computed for an energy injection source with a constant rate of 10^{15} J/s: (a) Pressure change at r=30 km and $z=z_s$, and (b) Spectrum of Figure 8a.

Comparing the spectral peaks in Figures 5 and 8, we observe that for the same equivalent source intensity, the acoustic mode in Figure 8 is about 3 times larger than that in Figure 5, and the gravity mode is about 60 times larger. Although this comparison is crude, it is useful for rough scaling of the results computed for mass injection sources to estimate the results for energy injection sources for which computation can be made only for a special case, $z=z_s$.

Eruption Time History

Equations (24), (25), and (29) give the pressure time history for a source for which the rate of mass or energy injection changes as a step function in time. If the rate of mass or energy injection is given by $\dot{m}(t)$ or $\dot{e}(t)$, respectively, the time history can be given by convolution of $\dot{m}(t)$ and $p_H(r,z,t)$ or $\ddot{e}(t)$ and $p_H(r,z,t)$, respectively. Here we use two types of eruption time histories:

$$\text{p0 source: } \dot{m}(t) \text{ or } \dot{e}(t) = (t/\tau^2)\exp(-t/\tau) \quad (30)$$

and

$$\text{p1 source: } \dot{m}(t) \text{ or } \dot{e}(t) = (t^2/2\tau^3)\exp(-t/\tau) \quad (31)$$

which are shown in Figure 9.

Figure 10 shows examples for an energy injection source computed with c=300 m/s, $z=z_s$, r=70 km, t=70 s, and $E_{total}=10^{15}$ J. These results can be directly compared with the result obtained from the LON record for the Mount St. Helens eruption. *Friedman et al.* [1981] estimated the total thermal energy released during the eruption of Mount St. Helens to be about 10^{17} to 10^{18} J. Figure 10 suggests that pressure changes of about 50 Pa (0.5 mbar) (p1 source) and 100 Pa (1 mbar) (p0 source) are expected at 1 hour after the eruption if the total energy is 10^{17} J. These estimates are in good agreement with the observed pressure change shown in Figure 3, considering the errors in the measurement and the simplicity of the model.

The large pulse labeled L in the beginning of the Longmire record shown in Figure 3 is the Lamb pulse studied by *Kanamori and Given* [1983]. This corresponds to the large pulse in the beginning of the computed

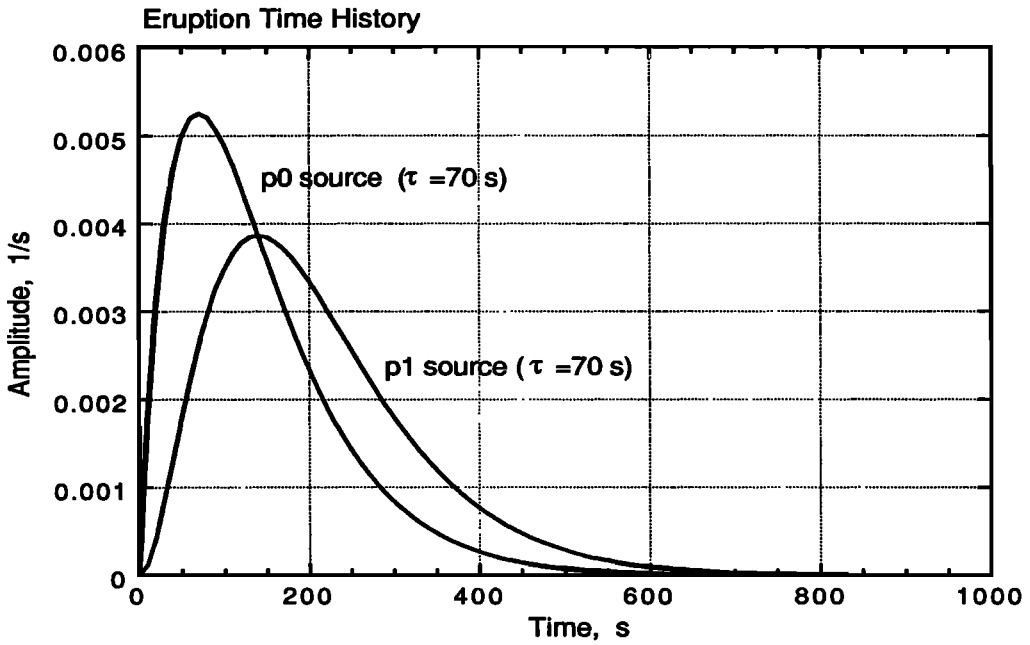

Figure 9. Two types of eruption time history.

pressure time histories shown in Figure 10. At far field, the Lamb pulse dominates so that the gravity waves that follow it would not be recognized. This is why all the previous studies were on the Lamb pulse only.

The energy release during a volcanic eruption is more complex than represented by the p0 and p1 sources. Nevertheless, the predicted pressure change, 50 to 100 Pa (0.5 to 1 mbar), is of the right order of magnitude. This result is encouraging in that a more detailed calculation using realistic models of eruption and the Earth's atmosphere will provide a good estimate of the total amount of eruption energy from seismological pressure measurements.

Since the eruption of Mount Pinatubo was a long continuous process, one would expect a complex turbulent thermal perturbation. However, a satellite image of Mount Pinatubo taken by the National Oceanic and Atmospheric Administration (NOAA) at 1030 GMT on June 15 indicates a relatively simple circular temperature perturbation associated with the eruption extending over a distance of 300 to 500 km from the summit (Figure 11) [*Matson et al.* 1991]. We computed the spatial variation of pressure as a function of distance using equations (24) and (25). The result is shown in Figure 12. In this computation we used a step function source; consequently, the pattern is relatively simple. Nevertheless, the overall feature of the satellite image could be reproduced.

Discussion and Conclusions

We have shown that atmospheric oscillations with about 100 Pa (1 mbar) amplitude can be excited by injection of energy of the order of 10^{17} J. This supports our primary conjecture that the thermal energy from the eruption and the acoustic and buoyancy restoring forces of the atmosphere are the cause of the observed oscillations.

We did not discuss the acoustic coupling between the atmospheric oscillations and seismic Rayleigh waves. However, the near vertical oscillation near the source can be modeled as a vertical single force. *Kanamori and Mori* [1992] showed that the amplitude of the observed Rayleigh waves is consistent with the pressure change of about 300 Pa (3 mbar) estimated for the Pinatubo eruption. We believe that this simple explanation is adequate to explain acoustic coupling.

As mentioned earlier, the near-source oscillations discussed in this paper decay more quickly than Lamb pulse so that only the Lamb pulse would be observed with a barograph placed at far field. In the Pinatubo case, the energy of the near-source oscillations was coupled to the ground near the source, propagated to far field, and observed with modern wide dynamic-range seismographs rather than barographs. In a way, the Earth as a whole worked as a barograph which detected near-source atmospheric oscillations. As shown by Figures 5a and 5b, the acoustic mode dominates near the source. Since the horizontal phase velocity of this mode is very large near the source, the energy couples to the ground efficiently. This is why the shorter-period acoustic mode dominates in the Pinatubo record, as shown in Figure 2. In contrast, a single peak at 300 s was observed for the Mount St. Helens and, possibly, the Krakatoa eruptions. In these cases, pressure waves rather than acoustically coupled seismic waves were directly recorded with a barograph at some distance away from the source, and only the longer-period gravity mode was observed. The gravity mode dominates when the observation point is some distance away, as shown by Figure 8.

The two peaks for the El Chichón eruption may be explained in the same way, but why the period of the shorter period mode is very different from that for the Pinatubo eruption is unclear.

The difference in the period between the longer period peak of the Pinatubo eruption and the Mount St. Helens

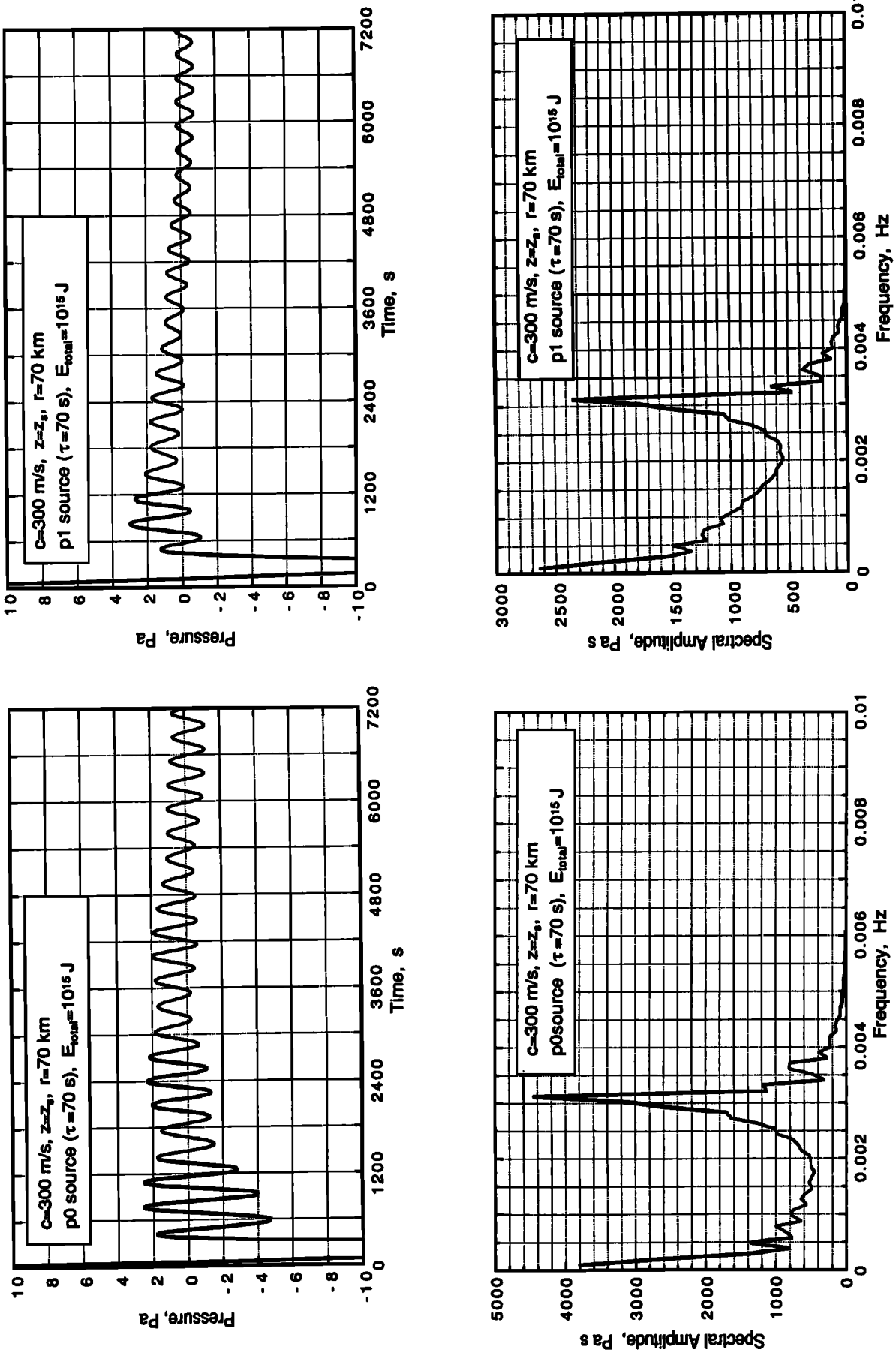

Figure 10. Pressure changes and their spectra for an energy injection source with p0 and p1 time histories shown in Figure 9.

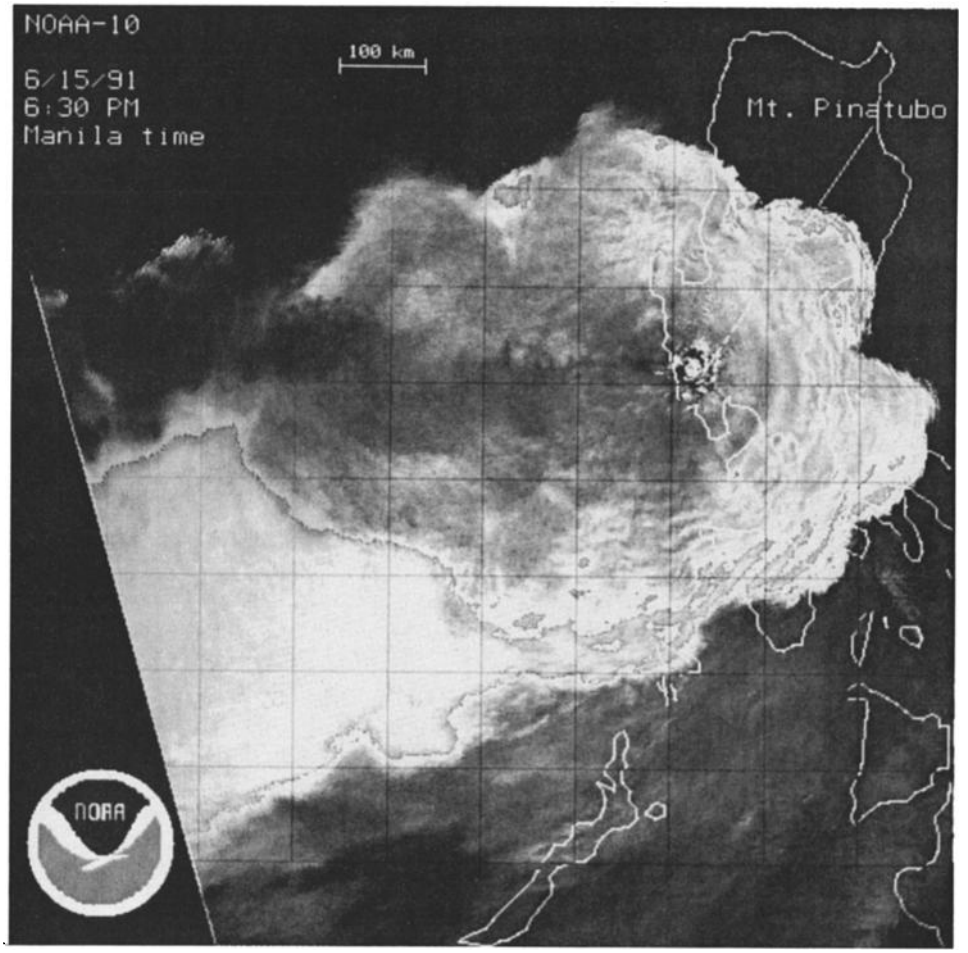

Figure 11. A satellite image of Mount Pinatubo taken by the National Oceanic and Atmospheric Administration (NOAA) at 1030 GMT on June 15 which indicates a circular temperature perturbation associated with the eruption extending over a distance of 300 to 500 km from the summit (made available by courtesy of NOAA).

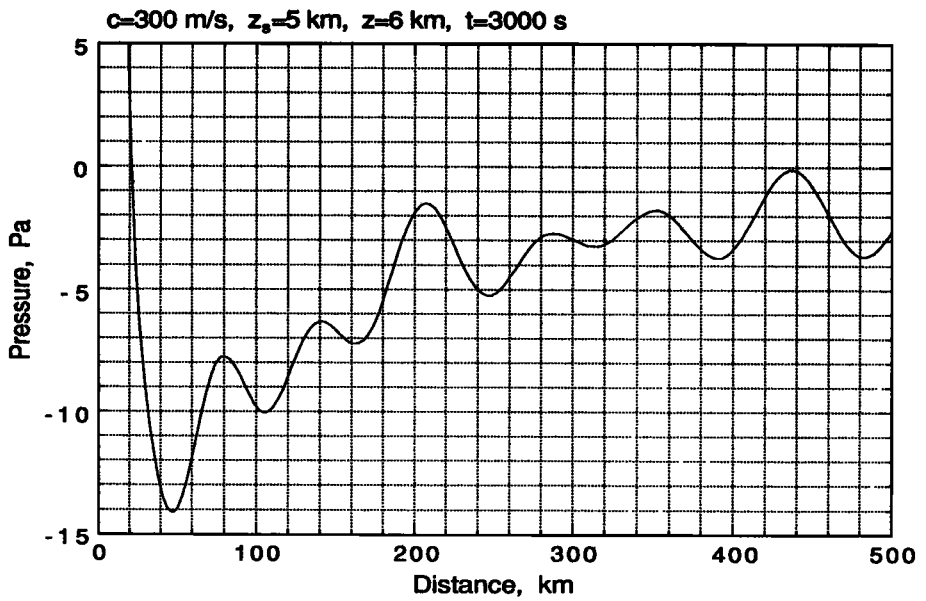

Figure 12. The spatial variation of pressure computed for the isothermal atmosphere.

eruption could be due to the difference in temperature and the effective density of the air, but no definitive conclusion can be made at present.

Although the present study is for a very simplified model of atmosphere and source, our results show that the model proposed by *Kanamori and Mori* [1992] is physically plausible, and suggest the possibility of using seismological methods for estimating the total energy release in volcanic eruptions and its effects on the Earth's atmosphere.

Appendix A: Solution for a Point Source

When the point sources given by (17) and (18) are added to (7) an (8), respectively, equations (9) and (10) become

$$\rho_0 \frac{\partial}{\partial t}\left(\frac{\partial w}{\partial z}-\frac{g}{c^2}w\right)=\left(\frac{\partial^2}{\partial x^2}+\frac{\partial^2}{\partial y^2}-\frac{1}{c^2}\frac{\partial^2}{\partial t^2}\right)p + 4\pi i\omega\left(F_M+\frac{F_E}{c^2}\right)\exp(i\omega t)\delta(\bar{R}-\bar{R}_s) \quad \text{(A1)}$$

and

$$\frac{\partial^2 w}{\partial t^2}-g\left(\frac{1}{\rho_0}\frac{\partial \rho_0}{\partial z}+g\frac{1}{c^2}\right)w=-\frac{1}{\rho_0}\frac{\partial}{\partial t}\left(\frac{\partial p}{\partial z}+\frac{g}{c^2}p\right) + 4\pi\frac{g}{c^2\rho_0}F_E\exp(i\omega t)\delta(\bar{R}-\bar{R}_s) \quad \text{(A2)}$$

respectively.

We introduce $\tilde{w}(x,y,z)$ and $\tilde{p}(x,y,z)$ by

$$w(x,y,z,t)=\tilde{w}(x,y,z)\exp(i\omega t)$$

and

$$p(x,y,z,t)=\tilde{p}(x,y,z)\exp(i\omega t) \quad \text{(A3)}$$

and substitution of (A3) in (A1) and (A2) obtains

$$\tilde{w}=\frac{i}{\omega h\rho_0}\left(\frac{\partial\tilde{p}}{\partial z}+\frac{g}{c^2}\tilde{p}\right)-\frac{4\pi g F_E}{\omega^2 h\rho_0 c^2}\delta(\bar{R}-\bar{R}_s) \quad \text{(A4)}$$

$$i\rho_0\omega\left(\frac{\partial\tilde{w}}{\partial z}-\frac{g}{c^2}\tilde{w}\right)=\nabla_H^2\tilde{p}+\frac{\omega^2}{c^2}\tilde{p}+4\pi i\omega F_M\delta(\bar{R}-\bar{R}_s) \quad \text{(A5)}$$

respectively, where

$$h=1-(\omega_b^2/\omega^2)$$

$$\omega_b^2=-g\left(\frac{1}{\rho_0}\frac{\partial\rho_0}{\partial z}+g\frac{1}{c^2}\right)$$

and

$$\nabla_H^2\equiv\frac{\partial^2}{\partial x^2}+\frac{\partial^2}{\partial y^2}$$

From (A4) and (A5), we obtain

$$\nabla_H^2\tilde{p}+\frac{1}{h}\left(\frac{\partial^2\tilde{p}}{\partial z^2}+\frac{\gamma g}{c^2}\frac{\partial\tilde{p}}{\partial z}+\frac{\omega^2}{c^2}\tilde{p}\right)= -4\pi i\omega\left[F_M+F_E\frac{1}{hc^2}\left(1+\frac{g}{\omega^2}\frac{\partial}{\partial z}\right)\right]\delta(\bar{R}-\bar{R}_s) \quad \text{(A6)}$$

Changing the dependent variable $\tilde{p}$ to $\tilde{p}/\rho_0^{1/2}$ reduces (A6) to

$$\nabla_H^2\left(\frac{\tilde{p}}{\rho_0^{1/2}}\right)+\frac{1}{h}\frac{\partial^2}{\partial z^2}\left(\frac{\tilde{p}}{\rho_0^{1/2}}\right)+\kappa^2\left(\frac{\tilde{p}}{\rho_0^{1/2}}\right)= -\frac{4\pi i\omega}{\rho_0^{1/2}}\left[F_M+F_E\frac{1}{hc^2}\left(1+\frac{g}{\omega^2}\frac{\partial}{\partial z}\right)\right]\delta(\bar{R}-\bar{R}_s) \quad \text{(A7)}$$

where

$$\kappa^2=\frac{\omega^2}{c^2}\left(\frac{\omega^2-\omega_a^2}{\omega^2-\omega_b^2}\right) \quad \text{(A8)}$$

If we introduce R^* by

$$R^{*2}=r^2+h(z-z_s)^2$$

$$r^2=x^2+y^2 \quad \text{(A9)}$$

(A7) can be written as

$$\frac{1}{R^{*2}}\frac{\partial}{\partial R^*}\left[R^{*2}\frac{\partial}{\partial R^*}\left(\frac{\tilde{p}}{\rho_0^{1/2}}\right)\right]+\kappa^2\left(\frac{\tilde{p}}{\rho_0^{1/2}}\right)= -\frac{4\pi i\omega}{\rho_0^{1/2}}\left[F_M+F_E\frac{1}{hc^2}\left(1+\frac{g}{\omega^2}\frac{\partial}{\partial z}\right)\right]\delta(\bar{R}-\bar{R}_s) \quad \text{(A10)}$$

Mass Injection Source

If we set F_E=0, then (A10) becomes

$$\frac{1}{R^{*2}}\frac{\partial}{\partial R^*}\left[R^{*2}\frac{\partial}{\partial R^*}\left(\frac{\tilde{p}}{\rho_0^{1/2}}\right)\right]+\kappa^2\left(\frac{\tilde{p}}{\rho_0^{1/2}}\right)= -\frac{4\pi i\omega F_M}{\rho_0^{1/2}}\delta(\bar{R}-\bar{R}_s) \quad \text{(A11)}$$

from which

$$p(r,z,t)=i\omega F_M\exp\left(-\frac{z-z_s}{2H_s}\right)\sqrt{h}\frac{1}{R^*}\exp(i\omega t\pm\kappa R^*)$$

$$p(r,z,t)=i\omega F_M\exp\left(-\frac{z-z_s}{2H_s}\right)\frac{(\omega^2-\omega_b^2)^{1/2}}{(\omega^2-\omega_c^2)^{1/2}}\frac{1}{R} \cdot\exp\left[i\omega\left(t\pm\frac{R}{C}\right)\right] \quad \text{(A12)}$$

where ω_c and C are given by (21).

To obtain (A12) from (A11), we noted that the solution of

$$\frac{1}{R^2}\frac{\partial}{\partial R}\left(R^2\frac{\partial\phi}{\partial R}\right)+k^2\phi=-4\pi\delta(\bar{R}-\bar{R}_s)$$

is given by

$$\phi=\frac{1}{R}\exp(\pm ikR)$$

Energy Injection Source

We set F_M=0 in (A10) and obtain

$$\frac{1}{R^{*2}}\frac{\partial}{\partial R^*}\left[R^{*2}\frac{\partial}{\partial R^*}\left(\frac{\tilde{p}}{\rho_0^{1/2}}\right)\right]+\kappa^2\left(\frac{\tilde{p}}{\rho_0^{1/2}}\right)=$$
$$-\frac{4\pi i\omega F_E}{\rho_0^{1/2}}\frac{1}{hc^2}\left(1+\frac{g}{\omega^2}\frac{\partial}{\partial z}\right)\delta(\bar{R}-\bar{R}_s) \quad \text{(A13)}$$

Comparing this with (A10), we obtain a particular solution in the form

$$p(r,z,t)=i\omega\frac{F_E}{\sqrt{h}c^2}\left(1+\frac{g}{\omega^2}\frac{\partial}{\partial z}\right)$$
$$\cdot\left[\exp\left(-\frac{z-z_s}{2H_s}\right)\frac{1}{R^*}\exp(i\omega t\pm\kappa R^*)\right]$$

This leads to equation (26).

Appendix B: Integrals in Equations (25) and (29)

The integral in equation (25) can be written more explicitly when the causality and radiation conditions are included.

$$\int_{-\infty}^{+\infty}\frac{(\omega^2-\omega_b^2)^{1/2}}{(\omega^2-\omega_c^2)^{1/2}}$$
$$\cdot\exp\left\{i\left[\omega t\pm\frac{(\omega^2-\omega_c^2)^{1/2}(\omega^2-\omega_a^2)^{1/2}}{(\omega^2-\omega_b^2)^{1/2}}t_0\right]\right\}d\omega$$
$$=2\int_0^{\omega_c}\frac{(\omega_b^2-\omega^2)^{1/2}}{(\omega_c^2-\omega^2)^{1/2}}$$
$$\cdot\exp\left\{-\frac{(\omega_c^2-\omega^2)^{1/2}(\omega_a^2-\omega^2)^{1/2}}{(\omega_b^2-\omega^2)^{1/2}}t_0\right\}\cos\omega t d\omega$$
$$-2\int_{\omega_c}^{\omega_b}\frac{(\omega_b^2-\omega^2)^{1/2}}{(\omega^2-\omega_c^2)^{1/2}}$$
$$\cdot\sin\left[\omega t-\frac{(\omega^2-\omega_c^2)^{1/2}(\omega_a^2-\omega^2)^{1/2}}{(\omega_b^2-\omega^2)^{1/2}}t_0\right]d\omega$$
$$+2\int_{\omega_b}^{\omega_a}\frac{(\omega^2-\omega_b^2)^{1/2}}{(\omega^2-\omega_c^2)^{1/2}}$$
$$\cdot\exp\left[-\frac{(\omega^2-\omega_c^2)^{1/2}(\omega_a^2-\omega^2)^{1/2}}{(\omega^2-\omega_b^2)^{1/2}}t_0\right]\cos\omega t d\omega$$
$$+2\int_{\omega_a}^{\infty}\frac{(\omega^2-\omega_b^2)^{1/2}}{(\omega^2-\omega_c^2)^{1/2}}$$
$$\cdot\cos\left[\omega t-\frac{(\omega^2-\omega_c^2)^{1/2}(\omega^2-\omega_a^2)^{1/2}}{(\omega^2-\omega_b^2)^{1/2}}t_0\right]d\omega$$

Similarly, the integral in equation (29) can be written as

$$\int_{-\infty}^{+\infty}\frac{\omega}{(\omega^2-\omega_b^2)^{1/2}}\left(1-\frac{g}{2\omega^2H}\right)$$
$$\cdot\exp\left\{i\left[\omega t\pm\frac{\omega(\omega^2-\omega_a^2)^{1/2}}{(\omega^2-\omega_b^2)^{1/2}}t_0\right]\right\}d\omega$$
$$=2\int_0^{\omega_b}\frac{\omega}{(\omega_b^2-\omega^2)^{1/2}}\left(1-\frac{g}{2\omega^2H}\right)$$
$$\cdot\sin\left[\omega t-\frac{\omega(\omega_a^2-\omega^2)^{1/2}}{(\omega_b^2-\omega^2)^{1/2}}t_0\right]d\omega$$
$$+2\int_{\omega_b}^{\omega_a}\frac{\omega}{(\omega^2-\omega_b^2)^{1/2}}\left(1-\frac{g}{2\omega^2H}\right)$$
$$\cdot\exp\left[-\frac{\omega(\omega_a^2-\omega^2)^{1/2}}{(\omega^2-\omega_b^2)^{1/2}}t_0\right]\cos\omega t d\omega$$
$$+2\int_{\omega_a}^{\infty}\frac{\omega}{(\omega^2-\omega_b^2)^{1/2}}\left(1-\frac{g}{2\omega^2H}\right)$$
$$\cdot\cos\left[\omega t-\frac{\omega(\omega^2-\omega_a^2)^{1/2}}{(\omega^2-\omega_b^2)^{1/2}}t_0\right]d\omega$$

In evaluating these integrals, the square-root singularities such as

$$\int_0^{\omega_b}\frac{F(\omega)}{(\omega_b^2-\omega^2)^{1/2}}d\omega$$

can be handled by changing the integration variable ω to $u=(\omega_b-\omega)^{1/2}$. Thus

$$\int_0^{\omega_b}\frac{F(\omega)}{(\omega_b^2-\omega^2)^{1/2}}d\omega=2\int_0^{\omega_b^{1/2}}\frac{F(\omega_b-u^2)}{(2\omega_b-u^2)^{1/2}}du$$

Acknowledgments. We thank Andy Ingersoll for helpful discussions which motivated us to conduct this study. Discussions with Don Anderson and Tom Heaton helped us improve our understanding of the eruption process. We thank Raymond Hide for enlightening discussion on the physics of atmospheric waves. Reviews by Toshiro Tanimoto and Rudolph Widmer contributed to improvement of the manuscript. We thank George Stephens and Mike Matson, who provided us with the satellite image shown in Figure 11. This research was partially supported by the National Science Foundation grant EAR-92 18809. This is contribution 5320, Division of Geological and Planetary Sciences, California Institute of Technology, Pasadena, California 91125.

References

Ben-Menachem, A., and S. J. Singh, *Seismic Waves and Sources*, 1108 pp., Springer-Verlag, New York, 1981.

Blanc, E., Observations in the upper atmosphere of infrasonic waves from natural or artificial sources: A summary, *Ann.Geophys.*, *3*, 673-688, 1985.

Bolt, B. A., and T. Tanimoto, Atmospheric oscillations after the May 18, 1980 eruption of Mount St. Helens, *Eos Trans. AGU, 62*, 529-530, 1981.

Brunt, D., The period of simple vertical oscillations in the atmosphere, *Q. J. R. Meteorol. Soc., 53*, 30-32, 1927.

Friedman, J. D., G. R. Olhoeft, G. R. Johnson, and D. Frank, Heat content and thermal energy of the June dacite dome in relation to total energy yield, May-October 1980, in *The Mullineaux*, pp. 557-567, U.S. Geological Survey, Washington, D. C., 1981.

Gill, A. E., *Atmosphere-Ocean Dynamics*, 662 pp., Academic, San Diego, Calif., 1982.

Harkrider, D. G., Theoretical and observed acoustic-gravity waves from explosive sources in the atmosphere, *J. Geophys. Res., 69*, 5295-5321, 1964.

Harkrider, D., and F. Press, The Krakatoa air-sea waves: An example of pulse propagation in coupled systems, *Geophys. J. Astron. Soc., 13*, 149-159, 1967.

Houghton, J. T., *The Physics of Atmospheres*, 2nd ed., 271 pp., Cambridge University Press, New York, 1986.

Jones, R. M., and T. M. George, Infrasound from convective storms, III, Propagation to the ionosphere, *J. Acoust. Soc. Am., 59*, 765-779, 1976.

Kanamori, H., and J. W. Given, Analysis of long-period seismic waves excited by the May 18, 1980, eruption of Mount St. Helens - A terrestrial monopole?, *J. Geophys. Res., 87*, 5422-5432, 1982.

Kanamori, H., and J. W. Given, Lamb pulse observed in nature, *Geophys. Res. Lett.,10*, 373-376, 1983.

Kanamori, H., and J. Mori, Harmonic excitation of mantle Rayleigh waves by the 1991 eruption of Mount Pinatubo, Philippines, *Geophys. Res. Lett., 19*, 721-724, 1992.

Kanamori, H., J. W. Given, and T. Lay, Analysis of seismic body waves excited by the Mount St. Helens eruption of May 18, 1980, *J. Geophys. Res., 89*, 1856-1866, 1984.

Lamb, H., *Hydrodynamics*, 6th ed., 738 pp., Dover, Mineola, N.Y., 1932.

Matson, M., G. Stephens, and J. S. Lynch, A satellite view of the Mount Pinatubo eruptions (abstract), *Eos Trans. AGU, 72* (44), Fall Meeting Suppl., 63, 1991.

Mikumo, T., and B. A. Bolt, Excitation mechanism of atmospheric-pressure waves from Mount St. Helens eruption, *Geophys. J. R. Astron. Soc., 81*, 445-461, 1985.

Pekeris, C. L., The propagation of a pulse in the atmosphere, *Proc. R. Soc., London A, A171*, 434-449, 1948a.

Pekeris, C. L., The propagation of a pulse in the atmosphere, II, *Phys. Rev., 73*, 145-154, 1948b.

Pfeffer, R. L., and J. Zarichny, Acoustic gravity wave propagation in an atmosphere with two sound channels, *Geofis. Pura Appl., 55*, 175-199, 1963.

Pierce, A. D., Propagation of acoustic-gravity waves from a small source above the ground in an isothermal atmosphere, *J. Acoust. Soc. Am., 35*, 1798-1807, 1963.

Press, F., and D. Harkrider, Propagation of acoustic-gravity waves in the atmosphere, *J. Geophys. Res., 67*, 3889-3908, 1962.

Press, F., and D. G. Harkrider, Air-sea waves from the explosion of Krakatoa, *Science, 154*, 1325-1327, 1966.

Row, R. V., Acoustic-gravity waves in the upper atmosphere due to a nuclear detonation and an earthquake, *J. Geophys. Res., 72*, 1599-1610, 1967.

Simkin, T., and R. S. Fiske, *Krakatau 1883*, 464 pp., Smithsonian Institution Press, Washington, D. C., 1983.

Väisälä, V., Über die Wirkung der Windschwankungen auf die Pilotbeobachtungen, *Commentat. Phys. Math. II, 19*, 1-46, 1925.

Weston, V. H., The pressure pulse produced by a large explosion in the atmosphere, *Can. J. Phys., 39*, 993-1009, 1961a.

Weston, V. H., The pressure pulse produced by a large explosion in the atmosphere, II, *Can. J. Phys., 40*, 431-445, 1961b.

Widmer, R., and W. Zürn, Bichromatic excitation of long-period Rayleigh and air waves by the Mount Pinatubo and El Chichón volcanic eruptions, *Geophys. Res. Lett., 19*, 765-768, 1992.

D. G. Harkrider and H. Kanamori, Seismological Laboratory 252-21, California Institute of Technology, Pasadena, CA 91125. (e-mail addresses: hark@seismo.gps.caltech.edu; hiroo@seismo.gps.caltech.edu)

J. Mori, U.S. Geological Survey, 525 S. Wilson Ave., Pasadena, CA 91106. (e-mail address: mori@bombay.gps.caltech.edu)

(Received October 8, 1993; revised May 23, 1994;
accepted June 8, 1994.)